Effect of spin diffusion on spin torque in magnetic nanopillars

Sergei Urazhdin and Scott Button
Department of Physics, West Virginia University, Morgantown, West Virginia 26506, USA
(Received 18 May 2008; revised manuscript received 10 October 2008; published 18 November 2008)

We present systematic magnetoelectronic measurements of magnetic nanopillars with different structures of polarizing magnetic layers. The magnetic reversal at small magnetic field, the onset of magnetic dynamics at larger field, and the magnetoresistance exhibit a significant dependence on the type of the polarizing layer. We performed detailed quantitative modeling showing that the differences are caused by the effects of spin-dependent electron diffusion.

DOI: 10.1103/PhysRevB.78.172403 PACS number(s): 75.47.De, 72.25.Ba, 72.25.Rb

Current-induced magnetic switching (CIMS) in nanoscale magnetic multilayers is caused by spin transfer (ST) from the conduction electrons to the magnetic layers, which occurs within atomic distances from the magnetic interfaces.[1] Nevertheless, electron diffusion in the layers can have a significant effect on ST.[2–4] For example, multiple electron scattering between two ferromagnets transfers angular momentum upon each reflection, while not significantly contributing to the net charge current I. Therefore, efficient utilization of electron scattering can reduce I required to manipulate magnetic devices. In a more subtle manifestation, spin-dependent electron diffusion causes an asymmetry between the ST in antiparallel (AP) and parallel (P) configurations of the magnetic layers,[5] in extreme cases leading to anomalous current-induced behaviors.[6]

Experimental studies of the effects of diffusion on ST (Refs. 6–10) have been hampered by the limited knowledge about the transport properties of individual layers and interfaces, which can significantly depend on the deposition techniques.[11] Since both the magnetoresistance (MR) and CIMS depend on the same spin-dependent transport properties, their simultaneous measurements and analysis within the same theoretical framework can lead to better understanding of the diffusion and its effect on ST. Here, we report on results for three multilayer structures elucidating different aspects of spin diffusion. Our calculations show that low-temperature results are consistent with the previously established transport properties of multilayers, while the temperature dependencies indicate that our present understanding of thermal spin-dependent scattering is inadequate.

Multilayers Cu(50)/F_1/Cu(10)/F_2/Cu(200) with identical free layers F_2=Py(5), Py=$Ni_{80}Fe_{20}$, and different polarizers F_1 were deposited at room temperature (RT) by magnetron sputtering at a base pressure of 5×10^{-9} Torr, in 5 mTorr of purified Ar. Thicknesses are in nanometers. F_1 was Co(20), Co(3), and $Fe_{50}Mn_{50}$(1)/Cu(1)/Co(3) in the three sample types labeled Co20, Co3, and FeMnCo3, respectively. Samples Co20 and Co3 allowed us to analyze the effects of spin diffusion in Co and the bottom Cu lead, respectively. Samples FeMnCo3 were not significantly affected by spin diffusion in F_1 due to the short spin diffusion length l_{sf} of FeMn.[11] F_2 and part of the Cu(10) spacer were patterned into a nanopillar with approximate dimensions of 130×60 nm^2, while F_1 was left extended with dimensions of several micrometers. A 30-nm-thick undoped Si layer insulating the leads was subsequently sputtered without breaking the vacuum to protect the nanopillar from oxidation, followed by deposition of a thick top Cu lead. We measured dV/dI with four-probe and lock-in detection. Positive I flowed from F_1 to F_2. Magnetic field H was in the film plane and along the nanopillar easy axis. At least three nanopillars of each type were tested.

Figures 1(a) and 1(b) show dV/dI vs I for a Co20 sample, acquired at RT and 5 K, respectively. The data at small $H=50$ Oe are characterized by hysteretic jumps to the P state with resistance R_P at $I^-<0$ and to the AP state with resistance R_{AP} at $I^+>0$. Large peaks appearing at $H=300/360$ Oe are caused by the reversible transitions between the AP state and a dynamical state with resistance above R_P. The onset of the magnetic dynamics at $I=I_C$ appears as a sharp increase in dV/dI nearly independent of H [1 kOe data in Figs. 1(a) and 1(b)]. The equality $I_C\approx I^+$ (dashed line) indicates that the reversal occurs when large-amplitude dynamics is excited by ST.[12] Figure 1(c) summarizes the T dependence of I^+ and I^-. Both dramatically decrease with increasing $T<130$ K, above which they remain nearly constant. A similar behavior was seen in Co/Cu/Co nanopillars.[8] Magnetic hysteresis remained square between 5

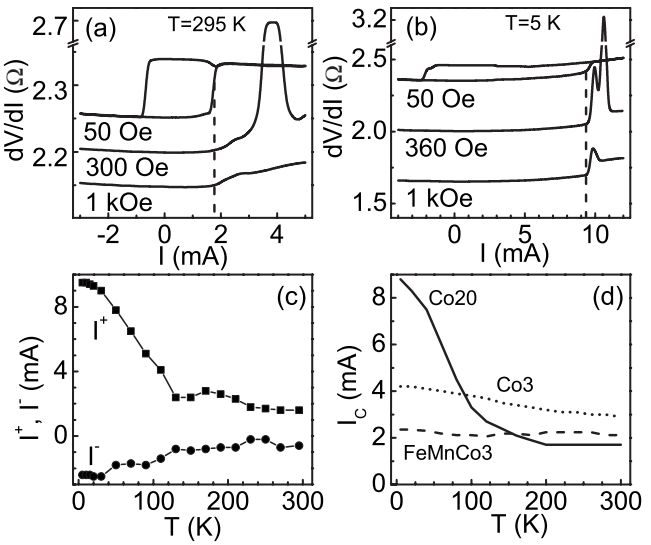

FIG. 1. (a) dV/dI vs I at labeled H and $T=295$ K. Curves are offset for clarity. (b) Same as (a), at $T=5$ K. (c) I^+ and I^- vs T for a Co20 sample. (d) I_C vs T measured at $H=500$ Oe for the three types of samples as labeled.

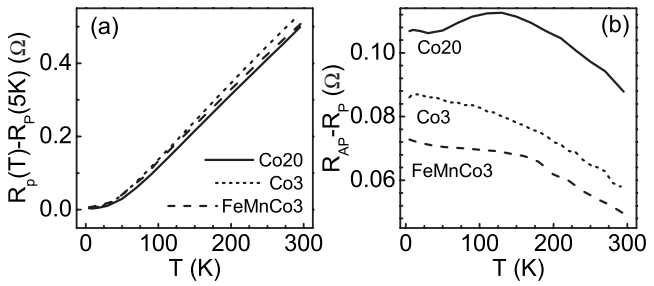

FIG. 2. (a) P-state resistances R_P offset by values at 5 K and (b) MR vs T for the three types of samples as labeled.

K and RT, eliminating magnetic inhomogeneity as the origin of these behaviors.

Some of the dependence on T in Fig. 1(c) may be caused by thermal activation. Therefore, we focus on the precession onset current I_C, which is a fundamental quantity predicted by the models, insensitive to thermal fluctuations and sample shape imperfections. It can be directly determined from the increase in dV/dI at H large enough to suppress hysteretic reversal. Additionally, inhomogeneity of F_1 is minimized at large H. Figure 1(d) summarizes I_C vs T for all three different sample structures. FeMnCo3 data are approximately independent of T, while I_C for Co3 and Co20 decreases with T. Comparing panels (c) and (d) reveals that I_C for Co20 closely follows I^+. It is not possible to measure a similar excitation onset current I_C^- in the AP state, because the stability of the P state is not suppressed at any H. Below, we use I^- as an approximation for I_C^-.

Since F_2 is identical in all samples, the different behaviors of I_C in Fig. 1(d) must be attributed to F_1. The difference between Co3 and FeMnCo3 is caused by the spin flipping in FeMn, which eliminates the spin diffusion in the bottom Cu(50) contact. The difference between the Co20 and Co3 data characterizes the effects of spin diffusion in Co vs Cu. We note that I_C is large in Co20 at low T, but it never diverges as would be expected if the sign of ST was reversed.[6]

Figures 2(a) and 2(b) show $R_P(T)-R_P(0)$ and $MR=R_{AP}-R_P$. The values of R_P increased with T due to the increased magnon and phonon scattering, and were surprisingly consistent among the samples. Interestingly, there is a clear correlation between the variations in MR and I_C. A decrease in MR in Co20 with increasing $T<130$ coincides with a sharp decrease in I_C. A slow decrease in MR in Co20 with increasing $T>130$ K and in other samples at all T is correlated with small variations in I_C.

To analyze the current-induced behaviors, we performed simultaneous calculations of spin-dependent transport and ST based on the model proposed by Slonczewski[5] and supported by Boltzmann-equation calculations.[13] To calculate I_C, we first derive the expression for ST in terms of the spin-dependent transport properties for collinear magnetic configuration, which can be determined in the diffusive Valet-Fert approximation.[14] From Eq. (28) of Ref. 5, the spin-torque per unit area of the F_2/N interface is

$$L_R = \hbar[\Delta J_L - \Delta J_R \cos\theta]/2e \sin\theta, \tag{1}$$

where ΔJ_L (ΔJ_R) is the difference between the spin-up and spin-down current densities in the Cu(10) spacer, in the reference frame determined by the magnetization of F_1 (F_2). Here, $\hbar$ is the Planck constant, e is the electron charge, and θ is the angle between the magnetizations of F_1 and F_2. Expressing J_R through J_L and a similarly defined spin accumulation ΔW_L via the spin-continuity equation (13) of Ref. 5, we obtain

$$L_R = \hbar \sin(\theta)(\Delta J_L - G\Delta W_L)/4e, \tag{2}$$

with $G \approx 1$ f Ω^{-1} m^{-2} estimated by Slonczewski for Co/Cu interfaces. The usual expression for ST per unit area is $\tau = \hbar j g(\theta) \sin\theta / e$,[1] where $g(\theta)$ characterizes the angular dependence of ST and j is the current density. Comparing to Eq. (2), we obtain $g(\theta) = (\Delta J_L - G\Delta W_L)/4j$. I_C is determined by $g(0)$,[1] which can be expressed in terms of the usual collinear transport parameters $j_s \equiv \Delta J_L(\theta=0)$ and $\Delta\mu \equiv \Delta W_L(\theta=0)$,[14]

$$I_C = 8\pi\alpha e M_2^2 V/(j_s/j - G\Delta\mu/j), \tag{3}$$

where $\alpha \approx 0.03$ is the damping parameter[15] and V is the volume of F_2. We determined the magnetization M_2 of Py by magnetometry of Py(5) films prepared under the same conditions as the nanopillars. It varied from 730 emu/cm^3 at 20 K to 675 emu/cm^3 at 300 K. The magnetization is lower than for bulk Py but consistent with the published data for films.[16] Extrapolation showed that M_2 at 20 K was close to its residual value at 5 K.

Equation (3) expresses I_C in terms of $\Delta\mu$ and j_s, the same quantities that determine MR in magnetic multilayers. I_C depends only on their ratios with j, which are independent of j in linear transport approximation. We calculated these ratios self-consistently using a one-dimensional diffusive Valet-Fert approximation employing the standard MR parameters: spin asymmetries β, renormalized resistivities $\rho^* = \rho/(1-\beta^2)$, spin diffusion lengths l_{sf} in the layers, and similarly defined parameters AR^*, γ, and δ for the interfaces.[14] We estimate these parameters from a combination of the published values[11] and our own measurements, as described below.

The resistivity $\rho(T)$ of each layer in our samples provides essential information about electron diffusion. Because of variations among published values, we instead determined ρ from measurements of thin films prepared under the same conditions as the nanopillars, with thicknesses verified by x-ray reflectometry. $\rho(T)$ was measured for 13-, 20-, and 40-nm-thick Py, Co, and Cu films at $T=5-300$ K. The dependence of the residual resistivity on film thickness was consistent with the Fuchs-Sondheimer approximation, allowing us to extract the bulk residual values $\rho_{Py}(0)=11.3$ $\mu\Omega$ cm, $\rho_{Co}(0)=4.4$ $\mu\Omega$ cm, and $\rho_{Cu}(0)=1.1$ $\mu\Omega$ cm. The dependence of ρ on T for Co and Cu was consistent with the Bloch-Gruneisen approximation, while Py data exhibited a quadratic dependence. In all cases, the dependencies on T were consistent among the films with different thicknesses, allowing us to estimate $\rho(T)$ for all the layers in the nanopillars.

To estimate $l_{sf}(T)$, we used its commonly assumed inverse relationship with ρ,[11] along with the bulk residual values $l_{sf,Py}(0)=6$ nm and $l_{sf,Cu}(0)=300$ nm based on published measurements,[11] scaled by the somewhat different residual resistivities of our films. If scattering by thermal excitations

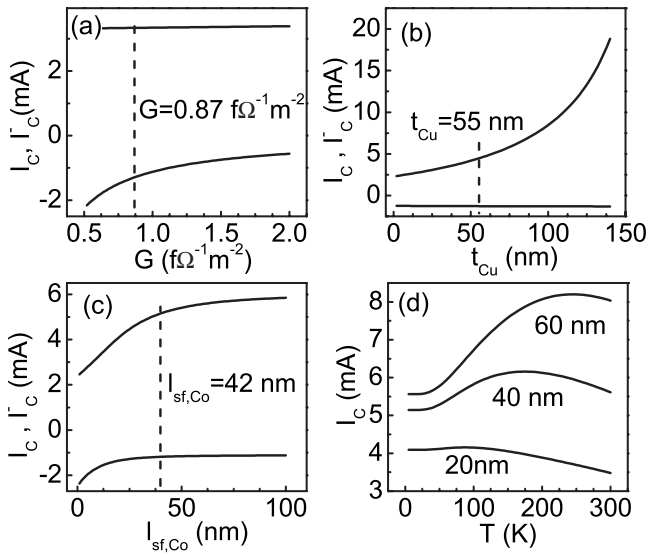

FIG. 3. (a) Calculated I_C and I_C^- vs G for FeMnCo3. (b) Same vs t_{Cu} for Co3. (c) Same vs $l_{sf,Co}$ for Co20. (d) I_C vs T for Co20 samples, for the residual values of $l_{sf,Co}$ as labeled.

does not flip electron spins, a weaker dependence $l_{sf}(T) \propto \sqrt{1/\rho(T)}$ is possible. However, we show below that a dependence even stronger than $1/\rho$ is more likely. We use $\beta_{Py}=\gamma_{Py/Cu}=0.7$, $\gamma_{Co/Cu}=0.8$, and $\beta_{Co}=0.36$ for spin asymmetries, $AR^*_{Co/Cu}=0.55$ f Ω m^2 and $AR^*_{Py/Cu}=0.5$ f Ω m^2 for renormalized interface resistances, and $\delta_{Co/Cu}=0.2$ and $\delta_{Py/Cu}=0.25$ for spin flipping coefficients.[8,11] Their dependence on T is neglected due to the dominance of the band structure and impurity scattering far from the Curie point. For FeMn, we used $l_{sf,FeMn} \approx 0.5$ nm, and $\rho_{FeMn}=87$ $\mu\Omega$ cm. Scattering at its interfaces was modeled by adding 0.5 nm to its nominal thickness. To account for the Cu contacts, the calculation included outer Cu layers of thickness t_{Cu} determined below. These layers were terminated with fictitious spin sinks.

To demonstrate that CIMS is extremely sensitive to the effects of diffusion, we now describe how our 5 K data can be fitted by appropriate choice of three parameters whose values have the largest uncertainty: conductance G in Eq. (2), effective MR-active thickness t_{Cu} of the Cu contacts, and spin diffusion length $l_{sf,Co}$. Calculations for FeMnCo3 were significantly affected only by G, which determines the asymmetry of CIMS. The values of $I_C/|I^-|$ in milliamperes measured at 5 K for three FeMnCo3 samples were 2.3/0.8, 1.6/0.6, and 3.1/1.5, giving an average ratio $I_C/|I^-|=2.5\pm0.2$. The calculated ratio increases from 1.46 at $G=0.5$ f Ω^{-1} m^{-2} to 6.1 at $G=2$ f Ω^{-1} m^{-2} [Fig. 3(a)]. The best approximation $I_C/|I_C^-|=3.34/1.27$ is obtained at $G=0.87$ f Ω^{-1} m^{-2}, in reasonable agreement with band-structure calculations.[5,17] We do not put uncertainty on this value because of the systematic errors introduced by the model and the uncertainties of other parameters.

Spin diffusion in the bottom Cu layer has little effect on Co20 and FeMnCo3 due to the spin relaxation in Co and FeMn, respectively. To determine t_{Cu}, we use the ratios $I_C/|I^-|$ for three Co3 samples, 3.55/1.0, 4.6/1.5, and 4.2/1.2, giving an average ratio $I_C/|I^-|=3.4\pm0.1$. The calculated

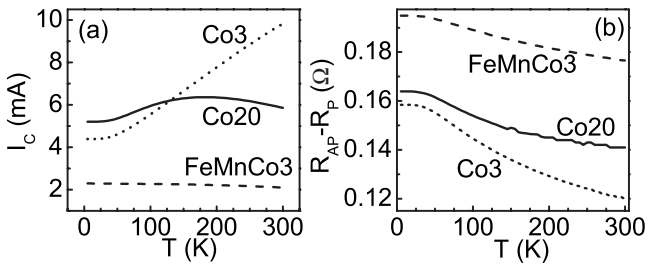

FIG. 4. (a) Calculated I_C vs T and (b) calculated MR vs T for three sample types as labeled.

$I_C/|I_C^-|$ increases from 1.9 for $t_{Cu}=0$ to 14 for $t_{Cu}=140$ nm [Fig. 3(b)] and eventually diverges at $t_{Cu}=200$ nm. The best agreement with data is obtained for $t_{Cu}=55$ nm, resulting in $I_C/|I_C^-|=4.4/1.3$.

Lastly, diffusion in Co significantly affects CIMS in samples Co20, but not in Co3 and FeMnCo3. We determine $l_{sf,Co}$ from the ratio $I_C/|I^-|$ for five Co20 samples, 8.9/2.1, 7.3/1.6, 9.0/2.0, 8.5/2.0, and 8.0/1.7, giving an average ratio $I_C/|I^-|=4.5\pm0.1$. Figure 3(c) illustrates that the calculated ratio $I_C/|I_C^-|$ increases from 1.0 for $l_{sf,Co}=0$ to 5.2 for $l_{sf,Co}=100$ nm. The best agreement with the data is obtained for $l_{sf,Co}=42$ nm consistent with the published values.[11]

Despite the ability to model the 5 K data, the calculations did not reproduce the dramatic dependence of I_C on T in Fig. 1 (see below). Therefore, one can attempt to determine $l_{sf,Co}$ from the dependence of I_C on T. Figure 3(d) shows calculations for the residual values $l_{sf,Co}=20$, 40, and 60 nm. Large $l_{sf,Co}$ results in I_C increasing with T, which is inconsistent with the data. Small $l_{sf,Co}$ results in I_C decreasing with T in better qualitative agreement with data but gives unreasonably small I_C at 5 K. We thus return to the value determined from Fig. 3(c).

Figures 4(a) and 4(b) present the calculated I_C and MR vs T for the three sample types. I_C for FeMnCo3 did not significantly depend on T, in agreement with the data. This result supports our assumption that the temperature dependence of scattering at Co/Cu interfaces is negligible. However, the calculations for Co20 and Co3 fail to even qualitatively reproduce the data: I_C increases with increasing $T<180$ K for Co20, and at all T for Co3, in contrast to the measured decreases for both sample types.

To better understand the implications of the differences between the data and the calculations, we note that I_C in Fig. 3 increased whenever the effective MR-active resistance R_1 of F_1 increased. For a single-layer F_1 with cross section A, $R_1=l_{sf}\rho/A$. For a multilayer F_1, R_1 is the sum of individual resistances weighed by the spin relaxation. For Co3 in Fig. 3(b), R_1 increased with increasing thickness of the Cu contact. For Co20 in Fig. 3(c), R_1 increased with increasing $l_{sf,Co}$ due to the contribution from the outer Co/Cu interface and the bottom Cu contact. A similar relationship between I_C and R_1 was established analytically.[5,18]

For Co3, the measured decrease in I_C with T indicates that R_1 decreases with T, implying that t_{Cu} must decrease. We originally assumed that, because of the large $l_{sf,Cu}$, this parameter is determined by the current spreading in the leads, which is a purely geometrical factor for a homogeneous ma-

terial. Data for Co3 thus suggest that thermal electron scattering in the Cu contact may change the effective geometry of the contact.

For Co20, the situation is more complicated, because R_1 is determined by a competition between the contribution of Co(20) increasing with T for $l_{sf,Co} > 20$ nm, and the contributions of the bottom Cu(50) contact and the outer Co/Cu interface, which decrease with T due to stronger spin flipping in Co(20). In calculations, the former dominates at $T < 180$ K, while the latter dominates at higher T, resulting in nonmonotonic $I_C(T)$. Both of these contributions to R_1 reduce the polarizing properties of F_1, lowering MR [Fig. 4(b)]. In contrast, the measured increase in MR and dramatic decrease in I_C with increasing $T < 130$ K suggest a significant reduction in R_1, and enhancement of the polarizing properties of F_1. To identify the origin of these behaviors, additional studies with different thicknesses of the polarizing Co layer may be warranted. Little is presently known about the temperature dependence of $l_{sf,Co}(T)$. We speculate that $l_{sf,Co}$ may decrease with T faster than $1/\rho_{Co}$, resulting in reduction in the $l_{sf,Co}\rho_{Co}$ contribution to R_1. The mechanism for such a rapid reduction in l_{sf} is presently unclear.

Our data may also indicate more fundamental limitations of the model. First, diffusive transport approximation may not adequately describe transport across heterostructures consisting of nanometer-scale layers. Second, the transport properties of our heterostructures may be modified by the nonequilibrium electron distribution during CIMS. Finally, the *s*-like and *d*-like components of the electron wave may have different contributions to the transport properties and CIMS. Nonequilibrium distribution calculations involving realistic band structures may be needed to address the significance of these effects.[19]

To summarize, we performed magnetoelectronic measurements of nanopillars with three different polarizing magnetic layers. The samples exhibited different current-induced behaviors attributed to the spin diffusion in the polarizing layer. The calculations reproduced the low-temperature behaviors with reasonable values of transport parameters. However, temperature dependencies of magnetoresistance and current-induced switching indicate that the effects of thermal scattering on spin transport are not yet well understood.

We thank Mark Stiles, Jack Bass, and Norman Birge for helpful discussions. This work was supported by the NSF under Grant No. DMR-0747609 and a Cottrell Scholarship from the Research Corporation.

[1] J. Slonczewski, J. Magn. Magn. Mater. **159**, L1 (1996).
[2] A. A. Kovalev, A. Brataas, and G. E. W. Bauer, Phys. Rev. B **66**, 224424 (2002).
[3] S. Zhang, P. M. Levy, and A. Fert, Phys. Rev. Lett. **88**, 236601 (2002).
[4] A. Shpiro, P. M. Levy, and S. Zhang, Phys. Rev. B **67**, 104430 (2003).
[5] J. Slonczewski, J. Magn. Magn. Mater. **247**, 324 (2002).
[6] O. Boulle, V. Cros, J. Grollier, L. G. Pereira, C. Deranlot, F. Petroff, G. Faini, J. Barnas, and A. Fert, Nat. Phys. **3**, 492 (2007).
[7] S. Urazhdin, N. O. Birge, W. P. Pratt, Jr., and J. Bass, Appl. Phys. Lett. **84**, 1516 (2004).
[8] T. Yang, A. Hirohata, M. Hara, T. Kimura, and Y. Otani, Appl. Phys. Lett. **89**, 252505 (2006).
[9] M. AlHajDarwish, H. Kurt, S. Urazhdin, A. Fert, R. Loloee, W. P. Pratt, Jr., and J. Bass, Phys. Rev. Lett. **93**, 157203 (2004).
[10] N. Theodoropoulou, A. Sharma, W. P. Pratt, Jr., and J. Bass, Phys. Rev. B **76**, 220408(R) (2007).
[11] J. Bass and W. P. Pratt, Jr., J. Magn. Magn. Mater. **200**, 274 (1999); J. Phys.: Condens. Matter **19**, 183201 (2007).
[12] S. Urazhdin, N. O. Birge, W. P. Pratt, Jr., and J. Bass, Phys. Rev. Lett. **91**, 146803 (2003).
[13] J. Xiao, A. Zangwill, and M. D. Stiles, Phys. Rev. B **70**, 172405 (2004).
[14] T. Valet and A. Fert, Phys. Rev. B **48**, 7099 (1993).
[15] I. N. Krivorotov, N. C. Emley, J. C. Sankey, S. I. Kiselev, D. C. Ralph, and R. A. Buhrman, Science **307**, 228 (2005).
[16] I. N. Krivorotov, N. C. Emley, A. G. F. Garcia, J. C. Sankey, S. I. Kiselev, D. C. Ralph, and R. A. Buhrman, Phys. Rev. Lett. **93**, 166603 (2004).
[17] K. Xia, P. J. Kelly, G. E. W. Bauer, A. Brataas, and I. Turek, Phys. Rev. B **65**, 220401(R) (2002).
[18] S. Urazhdin, R. Loloee, and W. P. Pratt, Jr., Phys. Rev. B **71**, 100401 (2005).
[19] P. M. Haney, D. Waldron, R. A. Duine, A. S. Nunez, H. Guo, and A. H. MacDonald, Phys. Rev. B **76**, 024404 (2007).